Available online at www.sciencedirect.com
ScienceDirect
Journal of Magnetic Resonance 187 (2007) 242–250
JMR Journal of Magnetic Resonance
www.elsevier.com/locate/jmr

# Low temperature probe for dynamic nuclear polarization and multiple-pulse solid-state NMR

HyungJoon Cho [a,1], Jonathan Baugh [b], Colm A. Ryan [b], David G. Cory [a], Chandrasekhar Ramanathan [a,*]

[a] Department of Nuclear Science and Engineering, Massachusetts Institute of Technology, Cambridge MA 02139, USA
[b] Institute for Quantum Computing, University of Waterloo, Waterloo, Ont., Canada, N2L 3G1

Received 8 January 2007; revised 4 April 2007
Available online 30 April 2007

**Abstract**

Here, we describe the design and performance characteristics of a low temperature probe for dynamic nuclear polarization (DNP) experiments, which is compatible with demanding multiple-pulse experiments. The competing goals of a high-Q microwave cavity to achieve large DNP enhancements and a high efficiency NMR circuit for multiple-pulse control lead to inevitable engineering tradeoffs. We have designed two probes—one with a single-resonance RF circuit and a horn-mirror cavity configuration for the microwaves and a second with a double-resonance RF circuit and a double-horn cavity configuration. The advantage of the design is that the sample is in vacuum, the RF circuits are locally tuned, and the microwave resonator has a large internal volume that is compatible with the use of RF and gradient coils.


*Keywords:* Dynamic nuclear polarization; Multiple-pulse NMR; Coherent averaging; Low temperature NMR

## 1. Introduction

NMR approaches to quantum information processing (QIP) have received much attention over the last decade. Liquid state NMR studies have explored the limits to controlling small quantum systems, and enabled the systematic study of open quantum systems. Solid-state NMR QIP approaches allow us to obtain control over a larger Hilbert space [1–6], and hold promise for the study of many body dynamics [7–11] and quantum simulations. Moreover, in the solid-state, the spins can be highly polarized by dynamic nuclear polarization techniques. The increased polarization allows an exploration of systems with a larger number of qubits, and also allows preparation of the system close to a pure state.

A number of solid-state NMR QIP experiments have recently been published [12–15], demonstrating that the coherent control necessary for QIP can be implemented in single crystal solids at room temperature. The next step is to take advantage of the high polarizations that are accessible in the solid-state. In order to reach high polarization via dynamic nuclear polarization (DNP) it is necessary to irradiate the system with microwaves, and to cool the sample down to liquid helium temperatures. The challenge here is to engineer the NMR probe so that these can be achieved without sacrificing high-fidelity control of the spins. In this paper we describe the design and performance characteristics of a low temperature probe for dynamic nuclear polarization experiments, which is also compatible with demanding multiple-pulse experiments.

Historically, DNP investigations have concentrated on two main areas: increased detection sensitivity of rare spins; and the creation of spin-polarized targets. The groups of Wind and Yannoni have explored a number of microwave resonator designs including horn-reflector [16],

* Corresponding author. Fax: +1 617 253 0760.
*E-mail address:* sekhar@mit.edu (C. Ramanathan).
[1] Present address: Schlumberger Doll Research, Cambridge, MA, USA.

1090-7807/$ - see front matter © 2007 Elsevier Inc. All rights reserved.
doi:10.1016/j.jmr.2007.04.012

Fabry–Perot [17], and cylindrical resonators [18] for DNP signal enhancement at room temperature. At lower temperatures Griffin and co-workers have implemented a novel design in which the cylindrical walls of a high-Q microwave cavity formed the RF coil for the NMR [19]. At even lower temperatures, the highest absolute polarizations reported were obtained using CW techniques in a multimode cavity in a dilution refrigerator [20].

The probe discussed here is designed for a top-loading continuous flow cryostat (spectrostatCF, Oxford Instruments) that fits in the bore of a 2.35 T superconducting magnet (89 mm bore diameter). The design specifications comply with the dimensional and functional aspects of this particular cryostat, but could easily be adapted to many other cryostats used in low temperature NMR applications. This field corresponds to an electron Larmor frequency of 66 GHz for $g = 2$. It is possible to obtain relatively inexpensive solid-state microwave sources with up to a Watt of power at this frequency. Fig. 1 shows a three-dimensional solid model of the main section of the probehead, as well as a cut-away view identifying the different components.

## 2. RF design

There is a wealth of experience in low temperature NMR [21–23]. There are two main challenges in the low temperature design of the tuned RF probe:

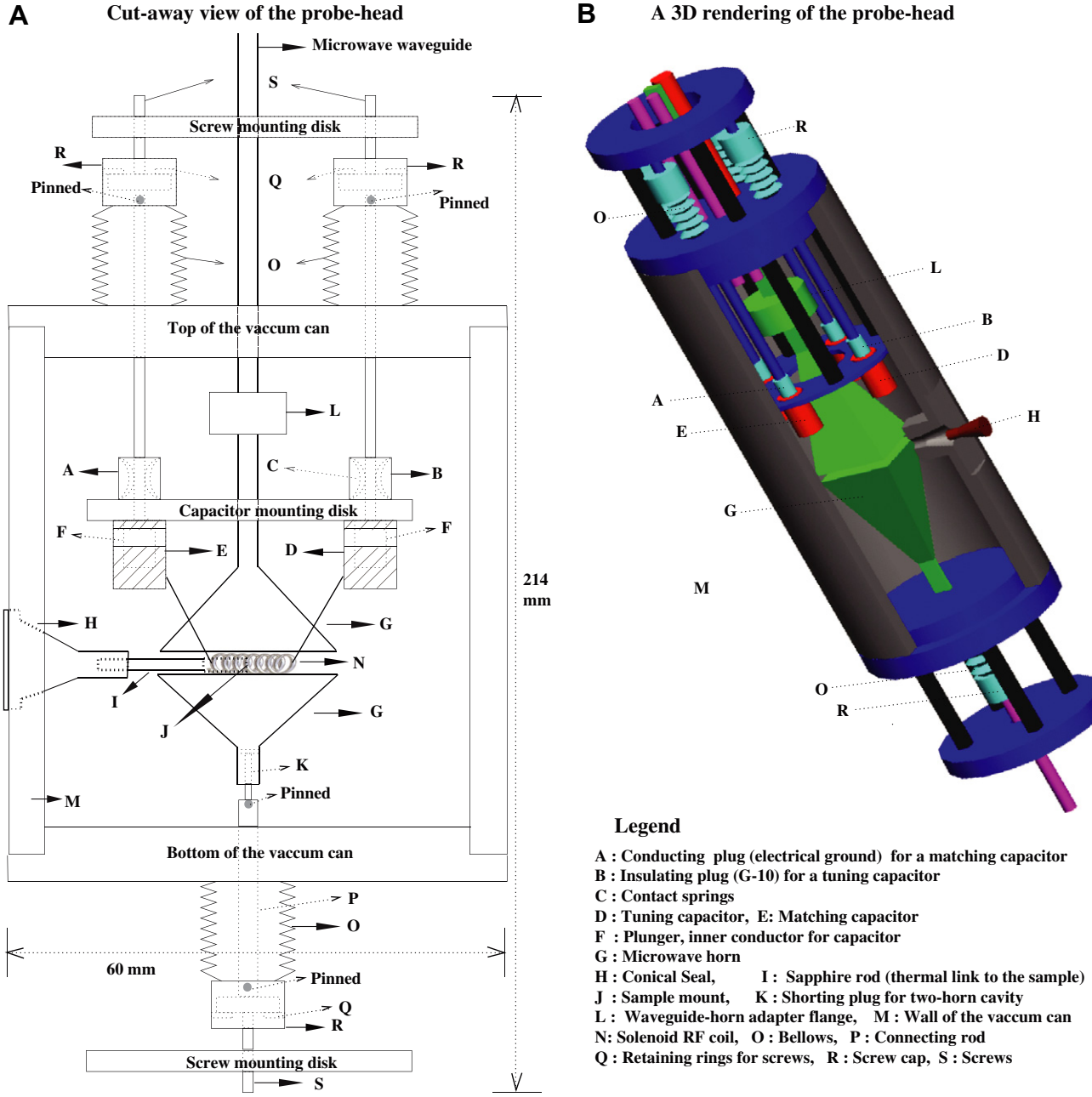


Fig. 1. Probe assembly: (A) cut-away view; and (B) three-dimensional CAD drawing.

- Maintaining the ability to tune and match the resonant circuit at low temperature.
- Ensuring that the sample remains at the desired operating temperature during the experiment.

As the probe is cooled down, the resonance invariably shifts due to contraction of the probe materials, and the $Q$ increases as the coil resistance is reduced. It is therefore necessary to re-tune and match the circuit once the operating temperature has been established. It is difficult to operate variable capacitors at low temperature as they have a tendency to seize if they have not been thoroughly cleaned. Although a simple approach to circuit tunability is to locate the tuning and matching elements outside the cryostat at room temperature, this entails a substantial loss of efficiency since a lossy transmission line becomes part of the resonant circuit [24–26]. An alternative approach that requires no tuning parts uses a large diameter coaxial line to reduce the losses [27]. However, space constraints and the need to reduce thermal losses up the coax limit the applicability of this solution, especially if multiple RF channels are needed. Our approach is to keep the tuning and matching capacitors at low temperature in close proximity to the sample coil.

The next challenge is to cool the sample itself down to the desired temperature. If the sample is in direct contact with the helium gas or liquid, the only requirement is that the sample temperature equilibrate to the bath. However, a tuned circuit in a gaseous $^4$He environment at low temperature is known to be susceptible to electric breakdown even at modest power levels. Although this may not be troublesome for a one-pulse experiment, high duty-cycle excitations such as spin-locking or multiple-pulse irradiation are likely to cause breakdown. The alternative is to locate the tuning circuit and RF coil, and usually the sample in a vacuum can evacuated to $\sim 10^{-5}$ torr. The sample is then mounted on a sapphire rod that is heat sunk at the other end to a copper plate. In this configuration we have found it difficult to cool the sample below about 6 K. The challenges are twofold. First we need to find a material that has high thermal conductivity as well as good dielectric properties at these temperatures. We used sapphire, which is a very good thermal conductor at low temperatures, though the conductivity peaks around 30 K and drops sharply below that [28]. Secondly we need to be able to place the sample in good thermal contact with this material. In our experiments, the quartz tube containing the frozen TEMPO solution was attached to the sapphire rod with Dow Corning vacuum grease.

An alternative solution is to seal the tuning circuit and the coil in a vacuum space, while the sample is immersed in helium. While this design permits both high RF powers and low sample temperatures, the tradeoff is a significantly smaller filling factor, resulting in lower $B_1$ fields compromising the resultant control [22,29].

### 2.1. RF transmission

In order to minimize conductive heat losses down the coaxial cables, we used UT-141C-SS semi-rigid coaxial cable (Micro-Coax), which has a silver-plated copper inner conductor and a stainless steel outer conductor with a PTFE dielectric. A series of brass baffles were used to minimize radiative losses to the room temperature flange. We have built two versions of the probe, a single-resonance probe tuned to protons, and a double-resonance probe tuned to protons and carbon. The standard circuit configurations used are shown in Fig. 2. We used standard tune-up sequences to calibrate the probes for multiple-pulse experiments. In order to minimize phase transients, we reduced the $Q$ of the circuits used. In the single-resonance probe we overcoupled the circuit, and in the double-resonance probe we added a 1.2 Ω metal oxide resistor, yielding a $Q$ of around 25.

A 3 mm diameter solenoidal RF coil was used in both probes, a 7-turn coil in the single-resonance circuit and a 9-turn coil in the double-resonance circuit. The wire was slightly flattened and then wound with a non-uniform pitch so as to optimize RF inhomogeneity [30]. The free-standing RF coil was supported by the leads as shown in Fig. 1.

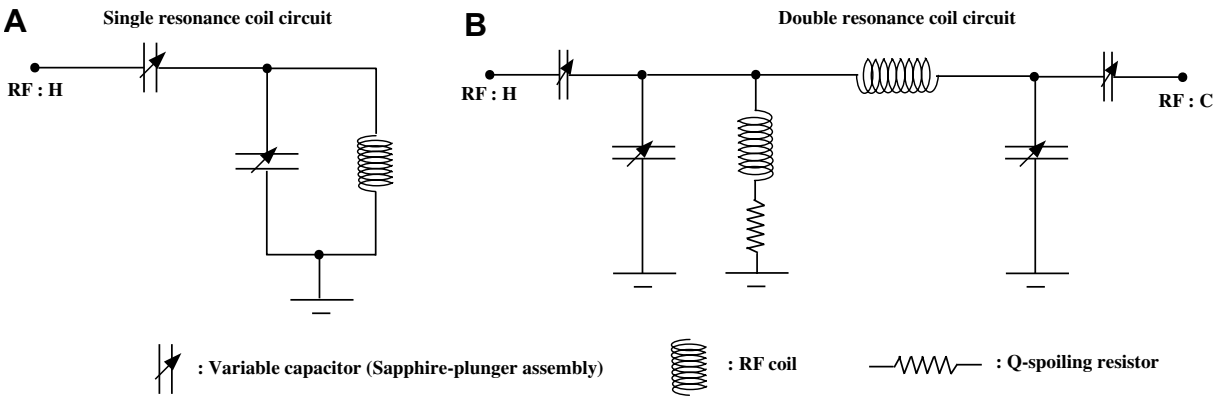


Fig. 2. Circuit schematics for the single- and double-resonance probes.

### 2.2. Tuning and matching

Fig. 3 shows a schematic diagram of the variable capacitor assembly. In order to achieve variable tuning and matching at low temperatures, we designed coaxial cylindrical capacitors using copper-plated sapphire tubes (7.8 mm OD, 4.8 mm ID, 14 mm in length) with a piston mechanism to obtain a capacitance range of 1–12 pF. The wall thickness of the sapphire dielectric is 1.5 mm, giving us a breakdown voltage of at least 25 kV. The capacitance range is obtained using $C = \epsilon\pi R_i^2 l/d \approx 10l$ pF (using $R_i = 4.8$ mm (ID of the sapphire tube), $d = 1.5$ mm (wall thickness of the tube), and where $l$ is the depth of the plunger in cm). The thickness of the copper plating is 50 μm, which is more than five times the skin depth of ~7 μm for copper at 100 MHz. We used a bellows mechanism (beryllium copper bellows, Mini-flex Corporation) to couple the room temperature rotary motion of the tuning rods to linear motion of the piston inside the low temperature vacuum can. A retaining ring (Rotor Clip, Inc.) was mounted inside the adapter on top of the bellows so that the bellows can be either extended or contracted by rotating a screw. Tuning rods made of G-10 extended to the room temperature flange at the top of the cryostat, where they passed through a set of Goddard quick-connect valves (Rego Products).

### 2.3. Sample cooling and orientation

To ease sample insertion and positioning, we machined a tapered conical seal (copper or brass) that doubles as a sample mount. Dow Corning silicone grease applied to the seal was found to be effective from room temperature to below 4 K. The advantage of using this approach is that one can easily change samples without opening a flange, and the (single crystal) sample orientation can be systematically varied by rotating the conical seal with respect to the vacuum can wall. A dial was inscribed onto the wall of the vacuum can to facilitate reproducible sample orientation. The conical seal also acts as a pressure release valve for the vacuum can, in the event of helium getting trapped inside the can. Fig. 4 shows a diagram of this conical seal. The sapphire rod attached to the conical seal extends to the center of the RF coil and the sample is mounted on the end of this sapphire rod. Clearly, efficient cooling of the sample by thermal contact is a critical issue for our vacuum can approach. Special care must be taken to ensure good thermal contact between the sample and the sapphire, and between the sapphire and the conical seal into which it is inserted. The external side of the conical seal makes contact with the gaseous $^4$He environment providing a cooling pathway for the sample.

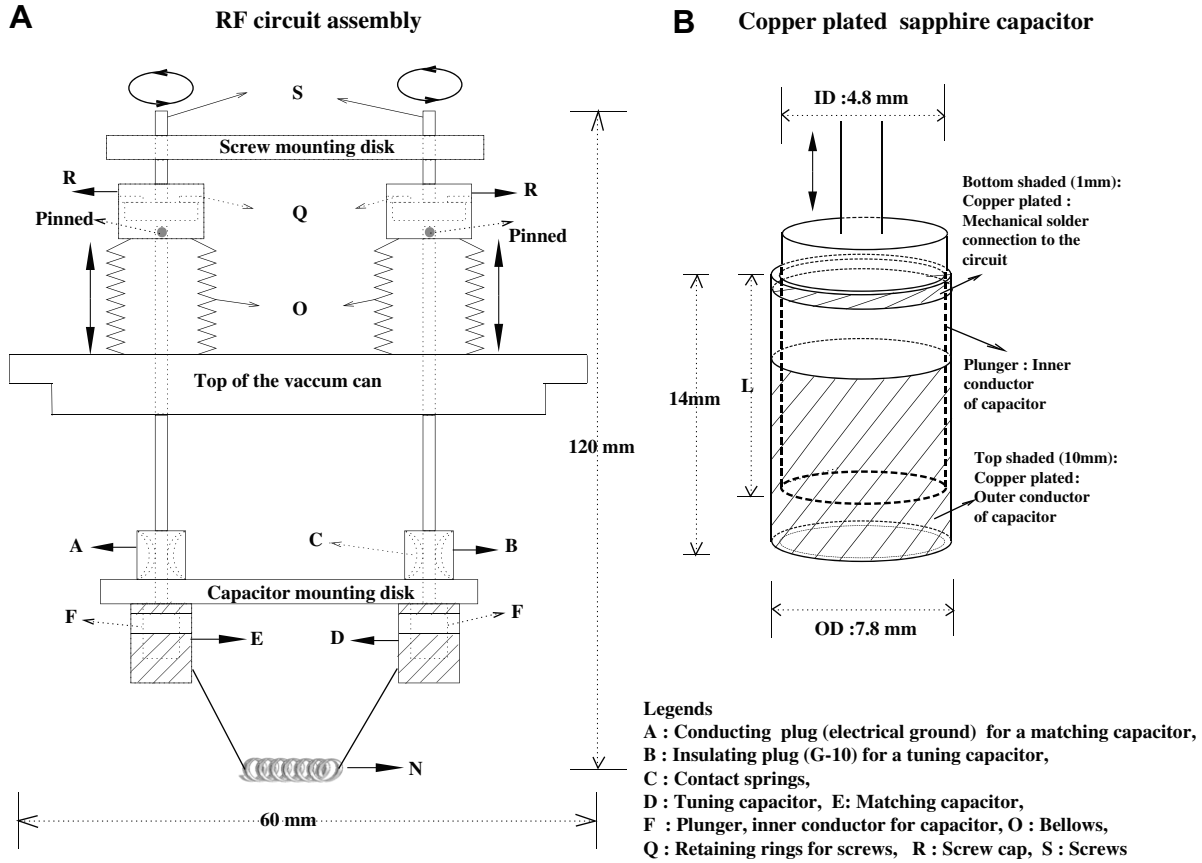


Fig. 3. (A) Schematic diagram of the variable capacitor assembly showing the copper-plated sapphire capacitors and the bellows arrangement that permits low temperature tuning inside the vacuum can. Rotary motion outside the can is converted to linear motion inside the can. (B) Detail of a single copper-plated sapphire capacitor.

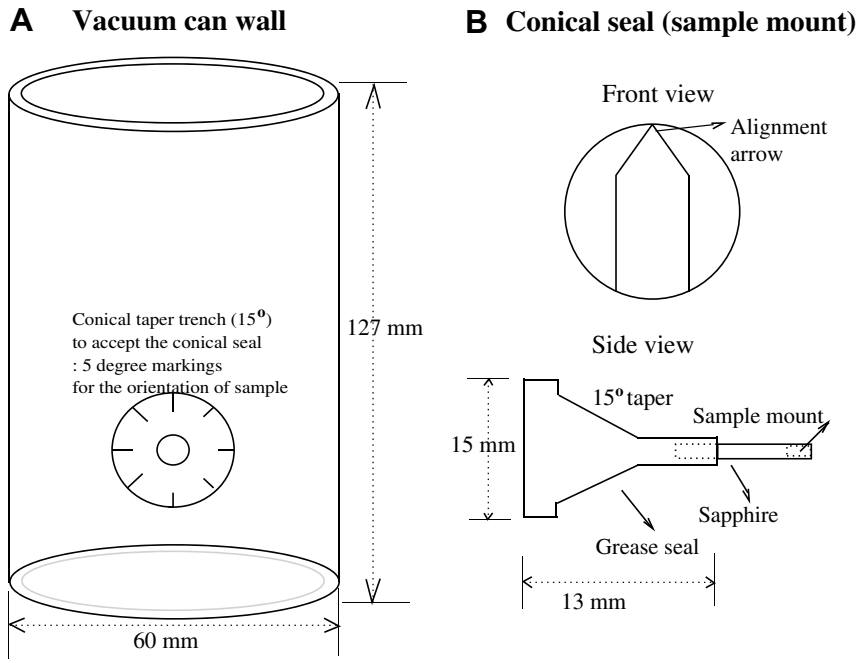


Fig. 4. (A) Side view of the wall of the vacuum can, showing the location where the conical seal sits, as well as the angular markings used to orient the sample. (B) Front and side views of the conical seal.

## 3. Microwave design

Microwave irradiation of the sample was achieved using microwave horns. A horn-mirror configuration was used in the single-resonance probe, and the double-horn configuration [31,32] was used with the double-resonance probe (Fig. 5). Although horn arrangements do not have particularly good microwave quality factors ($Q \sim 10$–$100$), they provide ample space to accommodate extra components such as RF and gradient coils. In addition they do not need any additional impedance matching arrangement. In the double-horn arrangement, the distance between the two horns was set equal to one wavelength of the microwave source so that the $3\lambda/4$ point (shown in Fig. 5) would have a minimum of the $E$-field on the horn surface. This allowed us to drill holes in the walls of the horn at this location, and pass the leads of the RF coil through the holes, without distorting the microwave mode structure. The shorter leads allow for greater RF efficiency.

Fig. 6 shows reflected power versus the relative distance of the mirror from the horn at 66 GHz microwave frequency, and similar data for the double-horn geometry (gap between the two horns is set to 4.5 mm, one wavelength at 66 GHz) as a function of a sliding shorting plug that is placed within the neck of the end horn. In the horn-mirror geometry, a loss of microwave power is observed as the gap between the horn and the mirror increases. The double-horn setup has a significantly higher quality factor ($Q \sim 100$) and shows reduced loss compared to the horn-mirror setup.

To effectively map out the $H$ field profile in the horn-mirror system, we performed HFSS (High Frequency Structure Simulator, AnSoft) simulations with the different horn configurations. Fig. 7 shows the simulated $H$ field profiles with the horn-mirror and double-horn geometries and a 66 GHz microwave source. We found that the horn-mirror and double-horn configurations have 4.5 dB and 7 dB gains in $H$ field strength, respectively, compared to a single horn.

### 3.1. Experimental setup

Fig. 8 shows a schematic of the experimental setup and the estimated insertion losses of the different components. We used a standard fundamental mode ($TE_{10}$) rectangular WR-15 waveguide to transmit the microwaves from the source to the cavity. The source used was a backshort-tuned Gunn oscillator (Millitech, LLC) with an attached isolator. Its center frequency is $66.2 \pm 0.1$ GHz with mechanical tuning ability of $\pm 2.0$ GHz. The available output power of this Gunn oscillator is 40–65 mW. We also performed experiments with two other sources, a 60 mW Gunn diode source from Millitech, LLC with a mechanical tuning range of $\pm 1.5$ GHz, and a 1 W source from Quinstar Technologies. The 1 W source was obtained by power combining the output of two impatt diode sources that are injection-locked with a Gunn to reduce phase noise. To connect the probe assembly and microwave source while maintaining vacuum inside the probe assembly, we used a bulkhead flange unit (Aerowave, Inc.) as a vacuum window on the top of low temperature NMR probe with mica and rubber O-ring seals. A mica window serves as a vacuum feed-through for microwave and has low insertion losses. To reduce microwave losses while maintaining thermal iso-

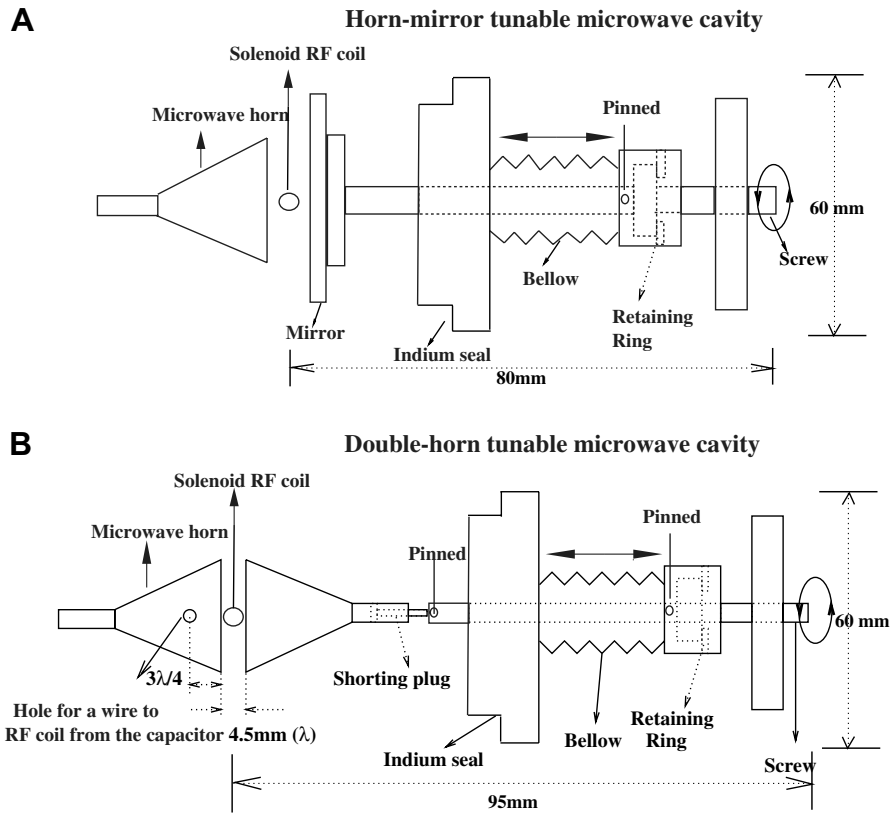


Fig. 5. (A) The horn-mirror arrangement showing the use of a bellows arrangement to move the mirror and tune the cavity from outside the vacuum can. (B) The double-horn arrangement showing the use of a shorting plug inserted into the second horn, that permits tuning. A pair of holes are placed in the upper horn, at a location where the *E*-field is minimum in order to minimize field distortions. Using these holes for the leads of the RF coil, minimizes the length and inductance of the leads, increasing coil efficiency.

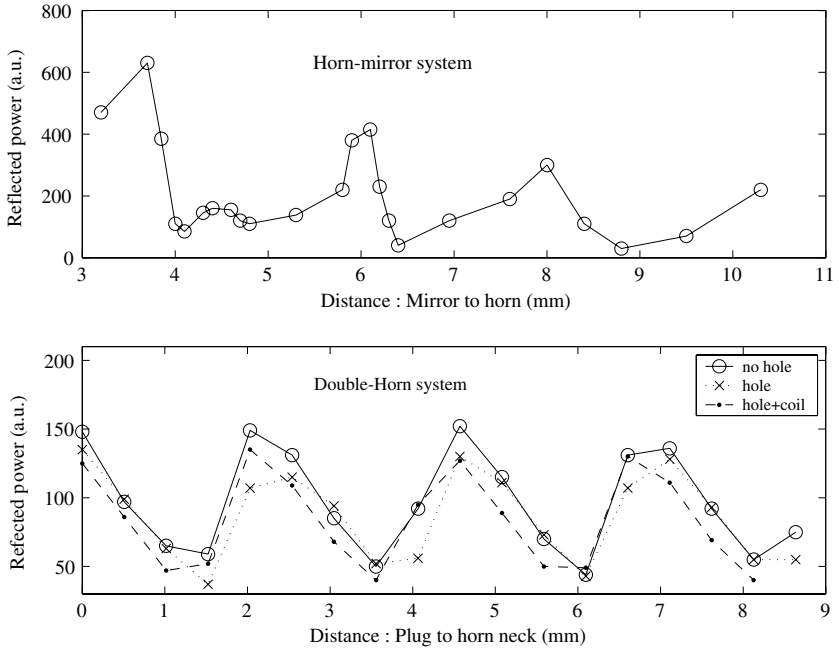


Fig. 6. Reflected power measurements for the two cavity geometries. In the lower figure, the *x*-axis shows the location of the shorting plug inside the neck of the horn.

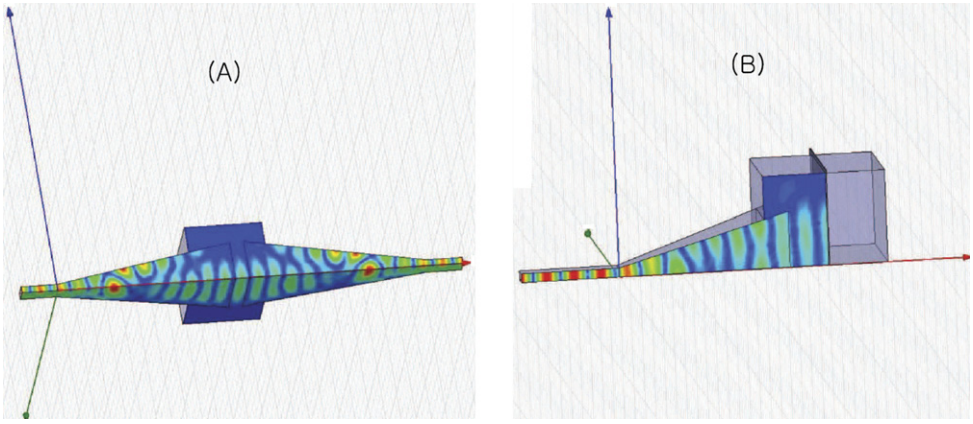


Fig. 7. HFSS simulations showing the $H$ field profiles in (A) the double-horn and (B) the horn-mirror cavity configurations.

lation between the sample area and the waveguide, a 4″ section of stainless steel waveguide was brazed into a 40″ long coin-silver waveguide. The stainless steel section acts as a heat switch limiting conduction up the waveguide. The total loss of microwave power was ~10.6 dB, resulting in ~5 mW output microwave power at the horn input. We do not always need to have the directional coupler in place, so we can save the 1.43 dB loss associated there.

In the single-resonance probe, the proton $\pi/2$ pulse was 1 μs with using a 300 W Bruker BLAX amplifier with 0 dBm input power. For the double-resonance probe, the measured $\pi/2$ pulses were 2 μs on both proton and carbon channels, using 300 W Bruker amplifiers on both channels, with 0 dBm input power.

## 4. Experimental results

DNP experiments were performed at 4 K and 2.35 T (100 MHz $^{1}$H, 25 MHz $^{13}$C), using a BRUKER Avance spectrometer and the home-built probes. A sample of 40 mM 4-amino-TEMPO radical (4-amino-2,2,6,6-tetramethylpiperidine 1-oxyl) in a 60/40 glycerol/water solution was used to test DNP. At this field strength and concentration, DNP is mediated by cross-relaxation between electron

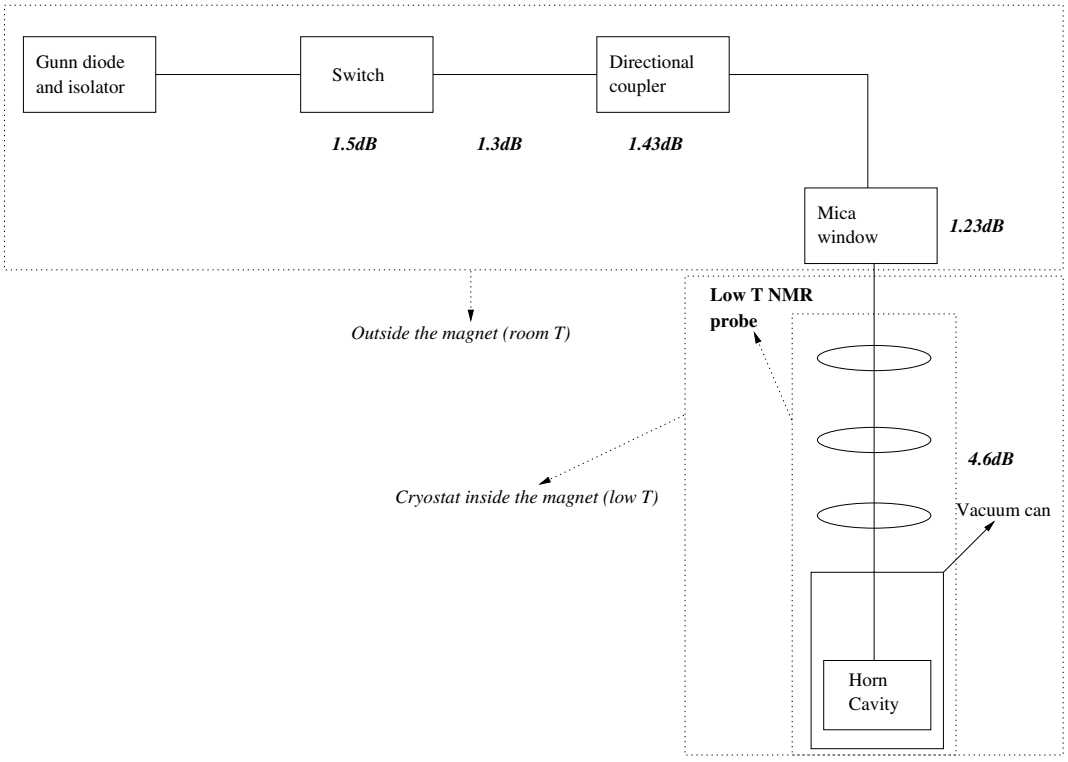


Fig. 8. A schematic drawing of the experimental setup. Estimated losses of microwave power due to waveguide sections and microwave elements are indicated in dB.

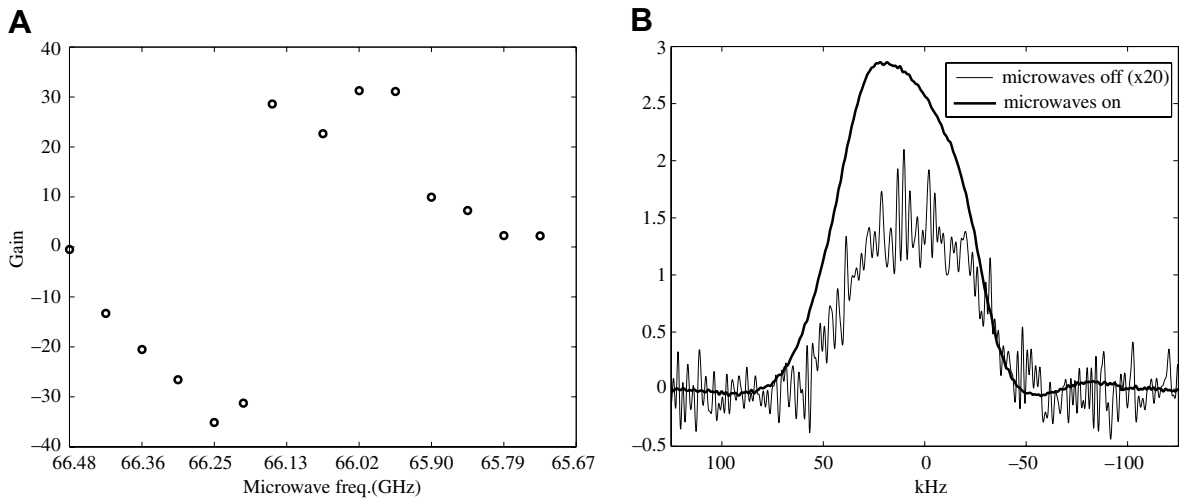


Fig. 9. (A) DNP enhancement of glycerol/water doped with 40 mM TEMPO as a function of microwave frequency, as obtained with a horn-mirror configuration. DNP is mediated by cross-relaxation between spin packets in the inhomogeneously broadened ESR line of TEMPO [33]. (B) DNP enhancement of 38 for the same system obtained with the double-horn configuration.

spins in the inhomogeneously broadened ESR line [33]. The sample volume was $\sim 2\ \text{mm}^3$. The 40 mM TEMPO solution is prepared by dissolving 0.05 g of 4-amino-TEMPO with a solution of 4.38 ml glycerol and 2.92 ml water. Fig. 9 shows the DNP enhancement obtained with the two probes. It is seen that experimentally the two cavities yield almost the same enhancement. This enhancement corresponds to a proton polarization of about 1.7%. With the double-resonance probe we were able to transfer this enhanced proton polarization to the carbon spins using Hartmann–Hahn cross-polarization. Fig. 10 shows the carbon signal enhancement following cross-polarization from the protons at 100 K and 6 K without DNP, and with DNP at 6 K.

Fig. 11 shows the proton spectra of the frozen gycerol/water solution obtained using a one-pulse experiment and an MREV-8 sequence [34]. It is seen that the single 70 kHz line seen in the one-pulse experiment is narrowed significantly and is about a kilohertz wide in the MREV-8 spectrum. The residual linewidth is most likely dominated by the proton CSA. Protons in ice are known to have an axially symmetric CSA ($\sigma_{\parallel} = 15 \pm 2$ ppm, $\sigma_{\perp} = -19 \pm 2$ ppm) [35]. The zero frequency peak in the MREV-8 spectrum corresponds to a residual spin-locking signal. In running the multiple-pulse experiments, the probe was initially tuned up at room temperature using a liquid sample, and the characteristic tuning curve of the probe measured. Following cool down to liquid helium temperatures, the

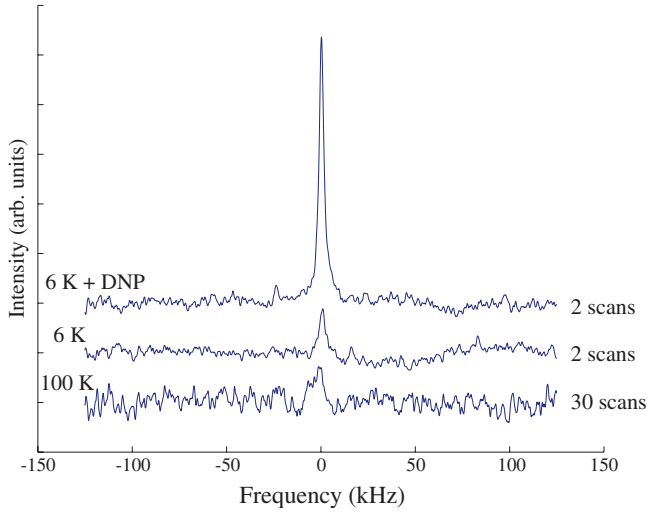


Fig. 10. $^{13}C$ spectrum of the frozen gycerol/water solution, showing the signal enhancement following proton DNP and cross-polarization from the protons to the carbon.

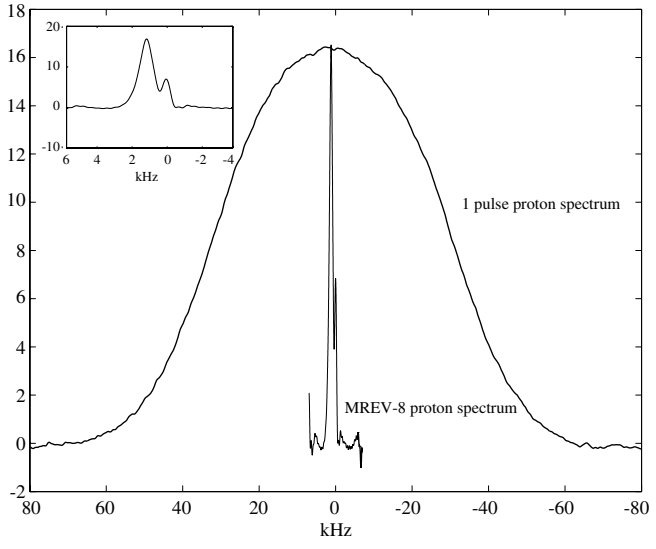


Fig. 11. One-pulse proton spectrum of the frozen glycerol/water solution, and a spectrum obtained with an MREV-8 sequence applied at a cryostat temperature of 4.2 K (sample temperature about 6 K). The inset shows the MREV-8 data expanded. The peak centered at 1.5 kHz corresponds to the water/glycerol signal, while the zero frequency peak is a residual spin-locking signal.

probe was re-tuned to try and match the measured room temperature characteristics.

We have shown that these probes can be used successfully to dynamically polarize the nuclear spins, and to implement both cross-polarization and multiple-pulse techniques. Additional modifications are possible to improve microwave performance, in particular by using overmoded waveguide to minimize losses during transmission to the cavity. Thermal losses could be minimized by using gold-plated stainless-steel waveguide. The sample in vacuum design ultimately limits the base sample temperatures achievable. We were able to reach a temperature of approximately 6 K. It is possible to lower this a little by improving the design, but as the thermal conductivity of sapphire drops sharply around 4 K, this design is unlikely to be useful at lower temperatures. At lower temperatures, a sample in helium design ensures that the sample reaches base temperature. If the RF electronics is maintained in liquid helium, arcing is prevented, and we are once again able to run high duty-cycle multiple-pulse experiments.

## Acknowledgments

We thank Peter Allen for his help in assembling the probes outlined here. This work was supported in part by the National Security Agency (NSA) under Army Research Office (ARO) contract numbers DAAD19-03-1-0125 and W911NF-05-1-0469, and by DARPA DSO and the Air Force Office of Scientific Research.

## References

[1] D.G. Cory, R. Laflamme, E. Knill, L. Viola, T.F. Havel, N. Boulant, G. Boutis, E. Fortunato, S. Lloyd, R. Martinez, C. Negrevergne, M. Pravia, Y. Sharf, G. Teklemariam, Y.S. Weinstein, W.H. Zurek, NMR based quantum information processing: achievements and prospects, Fortschr. Phys. 48 (2000) 875–907.

[2] G.P. Berman, G.W. Brown, M.E. Hawley, V.I. Tsifrinovich, Solid-state quantum computer based on scanning tunneling microscopy, Phys. Rev. Lett. 87 (2001) 097902.

[3] J. Wrachtrup, S.Y. Kilin, A.P. Nizovtsev, Quantum computation using the C-13 nuclear spins near the single nv defect center in diamond, Opt. Spectrosc. + 91 (2001) 429–437.

[4] D. Suter, K. Lim, Scalable architecture for spin-based quantum computers with a single type of gate, Phys. Rev. A 65 (2002) 052309.

[5] T.D. Ladd, J.R. Goldman, F. Yamaguchi, Y. Yamamoto, All-silicon quantum computer, Phys. Rev. Lett. 89 (2002) 017901.

[6] E. Abe, K.M. Itoh, T.D. Ladd, J.R. Goldman, F. Yamaguchi, Y. Yamamoto, Solid-state silicon NMR quantum computer, J. Supercond. 16 (2003) 175–178.

[7] W. Zhang, D.G. Cory, First experimental measurement of the spin diffusion rate in a homogeneous solid, Phys. Rev. Lett. 80 (1998) 1324–1327.

[8] G.S. Boutis, D. Greenbaum, H. Cho, D.G. Cory, C. Ramanathan, Spin diffusion of correlated two-spin states in a dielectric solid, Phys. Rev. Lett. 92 (2004) 137201.

[9] C. Ramanathan, H. Cho, P. Cappellaro, G.S. Boutis, D.G. Cory, Encoding multiple quantum coherences in non-commuting bases, Chem. Phys. Lett. 369 (2003) 311–317.

[10] H. Cho, T.D. Ladd, J. Baugh, D.G. Cory, C. Ramanathan, Multi-spin dynamics of the solid state NMR free induction decay, Phys. Rev. B 72 (2005) 054427.

[11] H. Cho, P. Cappellaro, D.G. Cory, C. Ramanathan, Decay of highly correlated spin states in a dipolar-coupled solid: NMR study of $CaF_2$, Phys. Rev. B 74 (2006) 224434.

[12] G.M. Leskowitz, N. Ghaderi, R.A. Olsen, L.J. Mueller, Three-qubit nuclear magnetic resonance quantum information processing sith a single-crystal solid, J. Chem. Phys. 119 (2003) 1643–1649.

[13] C. Ramanathan, S. Sinha, J. Baugh, T.F. Havel, D.G. Cory, Selective coherence transfers in homogeneous dipolar coupled spin systems, Phys. Rev. A 71 (2005) 020303.

[14] J. Baugh, O. Moussa, C.A. Ryan, A. Nayak, R. Laflamme, Experimental implementation of heat-bath algorithmic cooling using solid-state nuclear magnetic resonance, Nature 438 (2005) 470–473.

[15] J. Baugh, O. Moussa, C.A. Ryan, R. Laflamme, C. Ramanathan, T.F. Havel, D.G. Cory, Solid-state NMR three-qubit homonuclear system for quantum information processing: control and characterization, Phys. Rev. A 73 (2006) 022305.

[16] R.A. Wind, F.E. Anthonio, M.J. Duijvestijn, J. Smidt, J. Trommel, G.M.C. de Vette, Experimental setup for enhanced $^{13}C$ NMR spectroscopy in solids using dynamic nuclear polarization, J. Magn. Reson. 52 (1983) 424–434.

[17] D.J. Singel, H. Seidel, R.D. Kendrick, C.S. Yannoni, A spectrometer for EPR, DNP, and multinuclear high-resolution NMR, J. Magn. Reson. 81 (1989) 145–161.

[18] R.A. Wind, R.A. Hall, A. Jurkiewicz, H. Lock, G.E. Maciel, Two novel DNP-NMR probes, J. Magn. Reson. 110 (1994) 33–37.

[19] V. Weis, M. Bennati, M. Rosay, J.A. Bryant, R.G. Griffin, High-field DNP and ENDOR with a novel multiple-frequency resonance structure, J. Magn. Reson. 140 (1999) 293–299.

[20] W. de Boer, T.O. Niinikoski, Dynamic proton polarization in propanediol below 0.5 K, Nucl. Instrum. Methods 114 (1974) 495–498.

[21] M.S. Conradi, Low-temperature NMR techniques, Concepts Magn. Reson. 5 (1993) 243–262.

[22] P.L. Kuhns, S.H. Lee, C. Coretsopoulos, P.C. Hammel, O. Gonen, J.S. Waugh, A low temperature NMR probe for use in a dilution refrigerator, Rev. Sci. Instr. 62 (1991) 2159–2163.

[23] R.E. Norberg, W.L. Earl, Y.W. Kim, Cryogenic probe with low-loss transmission line for nuclear magnetic resonance, J. Magn. Reson. A 116 (1995) 139–144.

[24] J.H. Walton, M.S. Conradi, Probe-tuning adjustments—need they be in the probe? J. Magn. Reson. 81 (1989) 623–627.

[25] Y.W. Kim, W.L. Earl, R.E. Norberg, Cryogenic probe with low-loss transmission line for nuclear magnetic resonance, J. Magn. Reson. A 116 (1995) 139–144.

[26] V.D. Kodibagkar, M.S. Conradi, Remote tuning of NMR probe circuits, J. Magn. Reson. 144 (2000) 53–57.

[27] R.A. McKay, Double-tuned single coil probe for nuclear magnetic resonance spectrometer. US Patent 4,446,431, 01 May 1984.

[28] E.N. Smith, R.C. Richardson, Experimental Techniques in Condensed Matter Physics at Low Temperatures, Addison Wesley Publishing Company, Boston, 1998.

[29] A.Z. Damyanovich, J. Peternelj, M.M. Pintar, Design of a high-power NMR probe for low-temperature studies, J. Magn. Reson. 144 (2000) 1–5.

[30] R. Prigl, U. Haeberlen, The theoretical and practical limits of resolution in multiple-pulse high-resolution NMR of solids, Adv. Magn. Opt. Reson. 19 (1996) 1–58.

[31] E.S. Gravlin, J.A. Cowen, Simple microwave resonance spectrometer, Am. J. Phys. 27 (1959) 566.

[32] H. Nishiguchi, S. Sugito, N. Hirota, ESR spectrometers using electromagnetic horns, J. Magn. Reson. 68 (1986) 40–51.

[33] C.T. Farrar, D.A. Hall, G.J. Gerfen, S.J. Inati, R.G. Griffin, Mechanism of dynamic nuclear polarization in high magnetic field, J. Chem. Phys. 114 (2001) 4922–4933.

[34] U. Haeberlen, High Resolution NMR in Solids, Academic Press, New York, 1976.

[35] A. Pines, D.J. Ruben, S. Vega, M. Mehring, New approach to high-resolution proton NMR in solids: deuterium spin decoupling by multiple-quantum transitions, Phys. Rev. Lett. 36 (1976) 110–113.